Realizing the Potential of ZnO with Alternative Non-Metallic Co-Dopants as Electrode Materials for Small Molecule Optoelectronic Devices

Yong Hyun Kim, Jin Soo Kim, Won Mok Kim, Tae-Yeon Seong, Jonghee Lee, Lars Müller-Meskamp,* and Karl Leo*

High performance indium tin oxide (ITO)-free small molecule organic solar cells and organic light-emitting diodes (OLEDs) are demonstrated using optimized ZnO electrodes with alternative non-metallic co-dopants. The co-doping of hydrogen and fluorine reduces the metal content of ZnO thin films, resulting in a low absorption coefficient, a high transmittance, and a low refractive index as well as the high conductivity, which are needed for the application in organic solar cells and OLEDs. While the established metal-doped ZnO films have good electrical and optical properties, their application in organic devices is not as efficient as other alternative electrode approaches. The optimized ZnO electrodes presented here are employed in organic solar cells as well as OLEDs and allow not only the replacement of ITO, but also significantly improve the efficiency compared to lab-standard ITO. The enhanced performance is attributed to outstanding optical properties and spontaneously nanostructured surfaces of the ZnO films with non-metallic co-dopants and their straightforward integration with molecular doping technology, which avoids several common drawbacks of ZnO electrodes. The observations show that optimized ZnO films with non-metallic co-dopants are a promising and competitive electrode for low-cost and high performance organic solar cells and OLEDs.

1. Introduction

In recent years, there has been a rapid progress in the development of organic photovoltaic (OPV) cells with the power conversion efficiency reaching 12.0%.[1] Besides high efficiency, low-cost manufacturing is of great importance for realizing practical applications of OPV cells. Thus, significant efforts have been devoted to replacing indium tin oxide (ITO), which is the most common transparent electrode, due to its expensive price which results from limited supply of indium. Various alternative electrodes such as conductive polymer,[2,3] silver nanowire (AgNW),[4,5] carbon nanotube (CNT),[6] graphene,[7] and doped ZnO[8,9] have been widely investigated and show great potential. However, there are still several drawbacks to overcome. Poly(3,4-ethylenedioxythiophene): poly(styrenesulfonate) (PEDOT:PSS), CNT, and graphene are not as conductive as ITO and therefore lack in large area applications and AgNW networks are prone to cause leakage currents due to their inherent roughness.[4] Alternative oxide materials like doped ZnO suffer different drawbacks, i.e., a poor chemical stability under acidic PEDOT:PSS buffer layers.[10–12] Even though several studies based on these alternative electrodes have achieved device efficiencies comparable to ITO-based devices, very little could exceed it, so ITO is still regarded as the best performing electrode material for high efficiency OPV cells to date and remains the benchmark for all new technologies.

Doped ZnO films have been studied extensively and have the longest history among alternative electrode materials. Their low material cost, non-toxicity, high transmittance and high conductivity are great advantages. The electrical and optical properties of doped ZnO films have long reached those of ITO.[11] However, the chemical instability under acidic PEDOT:PSS typically used as a hole transport layer in polymer solar cells is still a critical issue, which significantly deteriorates the OPV performance.[10–12] Moreover, a low work function of ZnO films causes unfavorable energy level alignment, resulting in a hole injection problem.[8,13,14] For these reasons, the efficiency of ZnO-based OPV cells still lags behind that of ITO-based OPV cells.

Metallic elements such as aluminum and gallium are the most widely studied dopants on ZnO films, providing a high electrical conductivity. However, these films suffer from

Y. H. Kim, Dr. J. Lee, Dr. L. Müller-Meskamp, Prof. K. Leo
Dresdner Innovationszentrum für Energieeffizienz
Institut für Angewandte Photophysik
Technische Universität Dresden
01062 Dresden und Fraunhofer COMEDD
01109 Dresden, Germany
E-mail: lars.mueller-meskamp@iapp.de

J. S. Kim, Dr. W. M. Kim
Electronic Materials Research Center
Korea Institute of Science and Technology
39-1, Hawolgok-dong, Sungbuk-gu, Seoul 136-791, Republic of Korea
E-mail: wmkim@kist.re.kr

J. S. Kim, Prof. T.-Y. Seong
Division of Materials Science and Engineering
Korea University
Anam-Dong 5-1, Sungbuk-gu, Seoul 136-701, Republic of Korea

DOI: 10.1002/adfm.201202799

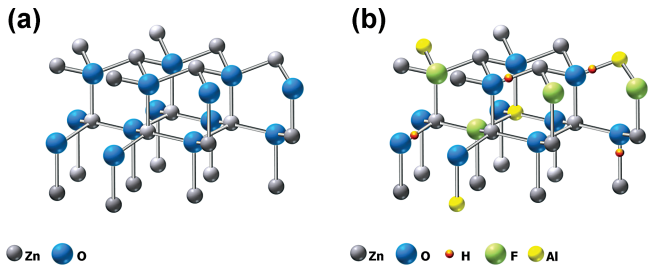

Figure 1. A schematic illustration of the a) intrinsic ZnO and b) co-doped ZnO hexagonal wurtzite structures, illustrating the different doping mechanisms: the electron rich Al atom substitutes a Zn lattice atom (the classic metallic doping) and, similarly, the electron rich fluorine replaces an oxygen atom, both donating an electron to the system. The hydrogen exists as single isolated interstitial bound with oxygen, thereby acting like fluorine and creating mobile charges.

significant optical absorption loss in near infra-red (IR) and visible range due to free carrier absorption, and strong perturbation of the conduction band from each metallic dopant. In contrast to metallic dopants, studies on anionic dopants such as fluorine are rare in spite of their possible benefit in producing ZnO films with high figure of merit in conjunction with low optical absorption loss.[15,16] Fluorine dopants substitute oxygen atoms whose orbitals dominate the valence band states. Therefore, fluorine donors have only little influence on the conduction band states, resulting in low free carrier scattering. In addition, a proper dose of fluorine dopants in the ZnO films has been reported to enhance the crystallization of ZnO and to reduce grain boundary scattering.[17] Another effective dopant in ZnO films is hydrogen. When doped, hydrogen is known to form an O-H complex which acts like an anionic dopant.[18,19] Hydrogen incorporated into ZnO films can increase the carrier concentration as well as passivate the grain boundaries.[20–22] Furthermore, our previous studies on ZnO or aluminum doped ZnO films co-doped with hydrogen and fluorine have shown that balancing the dopant contents and subsequent annealing could yield ZnO films with high figure of merit via counter acting mechanisms of hydrogen and fluorine.[20,21] A schematic illustration of the ZnO structures co-doped with non-metallic dopants and the acting mechanisms is presented in **Figure 1**.

In this study, we successfully produce high performance ZnO electrodes co-doped with alternative non-metallic dopants and report enhanced efficiencies in small molecule OPV cells and organic light-emitting diodes (OLEDs) using the alternative transparent conductive oxides (TCO). The optimized co-doping process of hydrogen and fluorine successfully reduces the metallic content of ZnO, which greatly improves the optical properties while retaining the high conductivity. Our experiments show that the optimized ZnO films are not only capable of replacing the ITO, but also improve the efficiency of the cells. The efficiency enhancement is the largest reported for OPV cells with alternative electrodes to our knowledge. The enhanced short circuit current densities and fill factors of OPV cells are due to optical effects of the ZnO with hydrogen and fluorine co-dopants and most probably additional morphological effects. The ZnO series exhibits lower optical losses and lower refractive indices compared to ITO, which allows excellent light in-coupling into the absorber layer. By using our organic doping technology, the integration of the different ZnO films for application in OPV cells is straightforward and does not show any adverse effects like charge injection/extraction barriers or interface resistances. Moreover, OLEDs based on optimized ZnO electrodes exhibit an enhanced light out-coupling efficiency due to reduced total internal reflection at the interface of the electrode and the organic layers.

Table 1. Fabrication details of TCO electrodes prepared by rf magnetron sputtering. Co-doping process is carried out by using carefully designed mixed target and mixed gas plasma.

TCO ID	Target	Working gas	Remark
ITO	–	–	Reference: purchased
ZnO:Al	ZnO-Al_2O_3(2 wt%)	Ar	
ZnO:H,F	ZnO-ZnF_2(10 wt%)	Ar-H_2(4 vol%)	
ZnO:Al,H,F	ZnO-Al_2O_3(1 wt%)	Ar-H_2(4 vol.%)-CF_4(0.4 vol%)	Annealed in vacuum at 300 °C

2. Results and Discussion

The fabrication details and electrical characteristics of the TCO films are summarized in **Table 1** and **Table 2**. The ZnO films are denoted as ZnO:X, where X indicates the dopants incorporated in films. The co-doping process is carried out based on previous experimental conditions by adjusting sputter gas composition as well as the target.[21] For a reliable comparison of the electrode effects on OPV cells and OLEDs, we tried to match the sheet resistances of the ZnO films with that of the ITO reference film by controlling the film thickness. Small differences in the values of sheet resistance are observed due to process variations, especially the nature of decreasing electrical resistivity with increasing film thickness of ZnO films, but those are in an acceptable range for reliable comparison between devices with small cell area.

Table 2. The electrical characteristics of TCO electrodes. All electrodes are designed to have similar sheet resistances. σ_{dc} and σ_{Op} are the dc and optical conductivities, calculated from transmittance and sheet resistance. $\sigma_{dc}\sigma_{Op}^{-1}$ values present a figure of merit for the electrodes used.

TCO ID	Thickness [nm]	Resistivity [$\times 10^{-4}$, Ω cm]	Hall mobility [$cm^2 V^{-1} s^{-1}$]	Carrier density [$\times 10^{20}$, cm^{-3}]	Sheet resistance [ohm sq^{-1}]	Work function [eV]	$\sigma_{dc}\sigma_{Op}^{-1}$
ITO	87	2.28	34.7	7.88	26.3	4.7	142
ZnO:Al	188	6.27	20.3	4.90	33.4	4.4	149
ZnO:H,F	596	14.9	24.4	1.72	24.9	4.3	166
ZnO:Al,H,F	205	4.97	23.8	5.27	24.3	4.5	283

Figure 2 shows transmittances, absorption coefficients, and refractive indices of the TCO electrodes used. At sheet resistances of around 24–33 ohm sq^{-1}, the average transmittances of ITO, ZnO:Al, ZnO:H,F, and ZnO:Al,H,F in the visible range of 400-800 nm are 83.3, 85.4, 84.1, and 87.2%, respectively. All ZnO films exhibit higher transmittances than the ITO reference. Since their sheet resistances are roughly equal, the highly transparent ZnO films are expected to be more favorable to the application of OPV cells. The striking feature in ZnO films with hydrogen and fluorine is the very low optical absorption loss as shown in Figure 2b. The average absorption coefficient of the ZnO:Al,H,F film is 703 cm^{-1} which is much lower than that of ITO (1724 cm^{-1}) in the visible range. The ZnO:H,F film fully doped with non-metallic contents shows an even lower absorption coefficient of 514 cm^{-1}. When ZnO thin films are fabricated in normal processing conditions, they are known to possess doubly charged defects such as zinc interstitials or oxygen vacancies, even in the presence of extrinsic dopants like aluminum or gallium. Those intrinsic and extrinsic defect centers increase in the optical absorption of thin films. Oxygen vacancies can be formed despite their high formation energy[23] and exist up to 400 °C.[24] Thus, the low absorption losses observed in hydrogen and fluorine co-doped ZnO films are attributed to the removal of oxygen vacancies by fluorine and a lower content of metallic elements.

Furthermore, the refractive index values of the ZnO series are lower than that of ITO, resulting in a reduced refractive index mismatch between the electrodes and the organic layers. Considering these properties, ZnO films are regarded as good alternative electrode material due to their excellent optical properties, i.e. higher transmittance, lower absorption loss, and lower refractive index compared to ITO. A figure of merit for transparent electrodes can be derived from the following equation, linking absorption and conductivity in thin, homogenous films:[3]

$$T = \left(1 + \frac{Z_0}{2R_S}\frac{\sigma_{Op}}{\sigma_{dc}}\right)^{-2} \quad (1)$$

where T is the transmittance, R_S is the sheet resistance, Z_0 (377 ohm) is the impedance of free space, and σ_{Op} and σ_{dc} are the optical and dc conductivities, respectively. The ratio of $\sigma_{dc}\sigma_{Op}^{-1}$ can be used as a figure of merit and the resulting values for the electrodes used in this study are shown in Table 2. As expected, the ZnO:Al,H,F film shows a much higher $\sigma_{dc}\sigma_{Op}^{-1}$ value (283) than ITO (142), indicating that optimized ZnO films are a superb material for the highly transparent and conductive electrode.

Since the properties of OPV cells are often known to be influenced by the electrode surface microstructure, the surface characteristics of ZnO electrodes are investigated by atomic force microscopy (AFM). The AFM images show clear differences in the surface topography of the different kinds of TCO electrodes as shown in **Figure 3**. The ITO film exhibits a very smooth surface with large, planar grains of several hundred nanometers in size. In contrast to ITO, a rough surface with fine granular structures is observed in the case of the ZnO:Al film. The ZnO:H,F and ZnO:Al,H,F films exhibit an even rougher surface along with round grains and densely distributed high

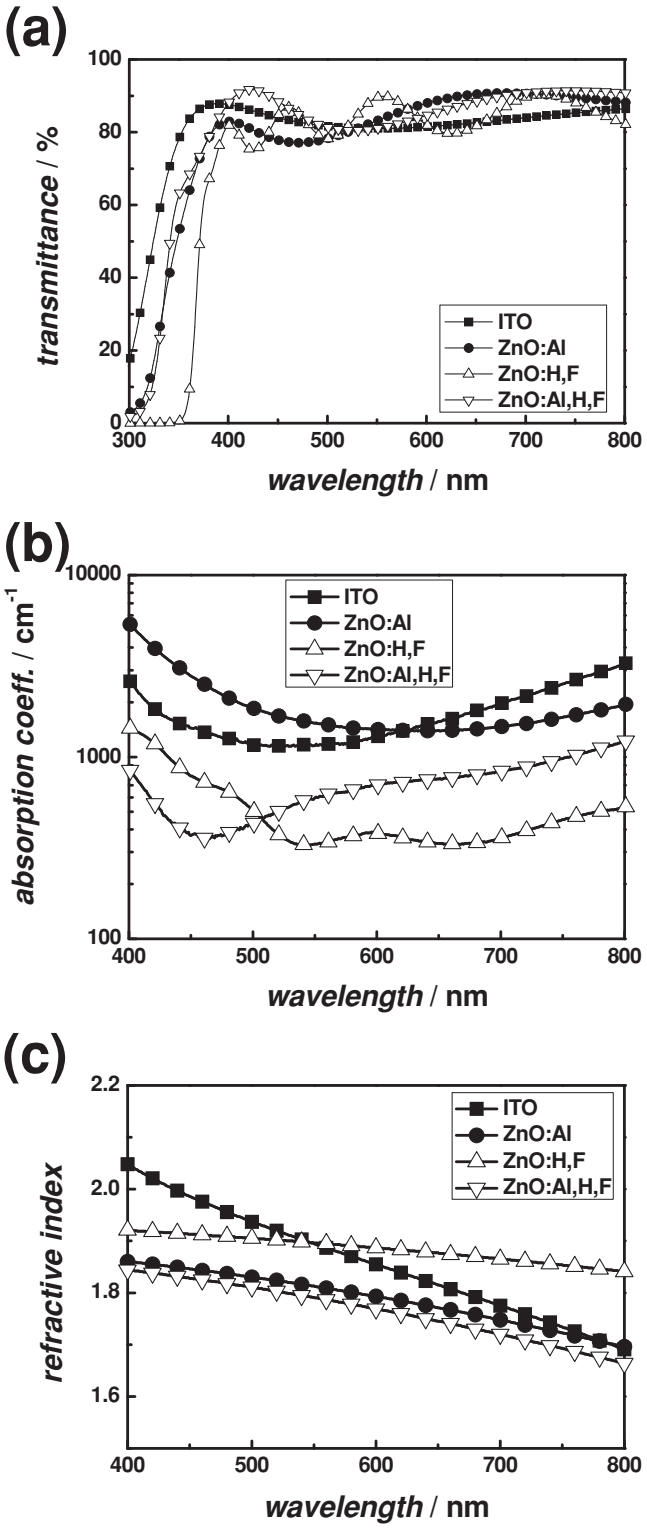

Figure 2. a) Transmittances (including the glass substrate), b) absorption coefficients, and c) refractive indices of TCO electrodes. ZnO films doped with hydrogen or fluorine show excellent optical properties such as higher transmittances, lower absorption coefficients, and lower refractive indices compared to ITO. All electrodes have roughly equal sheet resistances.

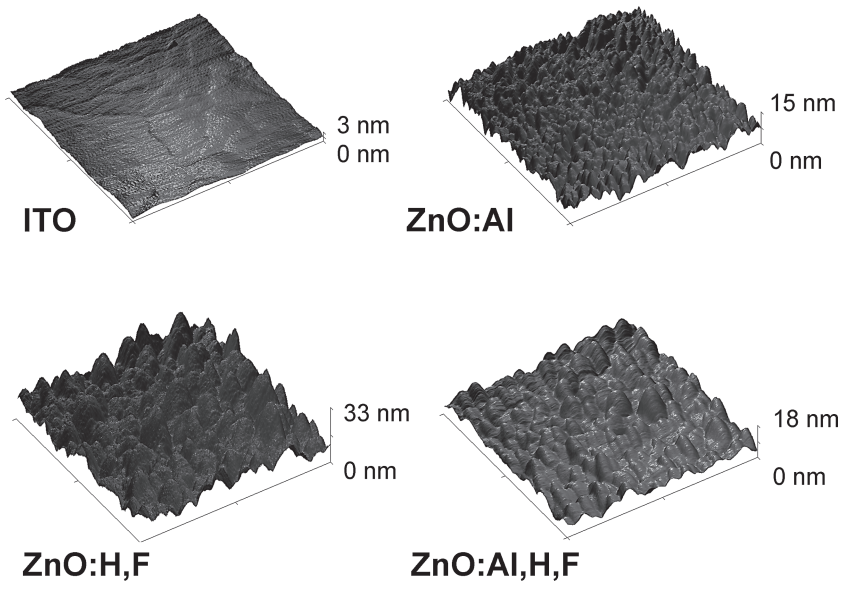

Figure 3. Topography images of TCO electrodes (1 × 1 μm^2). ZnO films co-doped with hydrogen and fluorine show spontaneously textured rough surfaces while the ITO film has a very smooth surface.

peaks. These spontaneously formed nano-structures have a size of tens of nanometers. The molecular orientation, crystallinity, and quality of the donor/acceptor junction of OPV cells are significantly affected by an underlying layer (i.e., bottom electrode or buffer layer).[25–28] The photovoltaic performances are expected to be influenced by the observed differences in surface morphology, which will be discussed later.

Having investigated the TCO properties, we fabricate p-i-i (p-doped, intrinsic, intrinsic layer) type small molecule OPV cells, carefully optimized for high efficiency. As an absorber layer, a fluorinated zinc phthalocyanine:fullerene (F4-ZnPc:C_{60}) bulk heterojunction is used. ZnPc and C_{60} are commonly used donor and acceptor materials in the small molecule OPV community. The F4-ZnPc used in this work is modified by fluorination, giving a higher open circuit voltage (V_{OC}) compared to pure ZnPc as reported recently.[29] The blend layer is heated at 100 °C for better crystallinity and nanomorphology, resulting in improved fill factors (FF) and short circuit current densities (J_{SC}). The hole transport layer (HTL) is doped with a p-dopant and a very thin p-dopant layer is introduced at the interface between electrode and HTL to achieve an ohmic contact with a negligible hole extraction barrier, showing more efficient carrier transport properties.[2,30] Thanks to the interface doping, the common problem of an energy level mismatch between highest occupied molecular orbital (HOMO) of the HTL and ZnO does not affect our system. This allows us to avoid PEDOT:PSS and the associated chemical instability in combination with the ZnO. An intrinsic C_{60} layer is deposited on the absorber blend layer for additional light absorption and electron transport. 4,7-diphenyl-1,10-phenanthroline (BPhen) is used as an exciton blocking layer to prevent exciton quenching and damage of cathode deposition. All OPV cells are fabricated in one run, enabling a reliable comparison of the influence of electrodes. The devices are denoted as OPV_X, where the subscripts of X indicate the type of bottom electrodes used such as ITO, ZnO:Al, ZnO:H,F, and ZnO:Al,H,F. In **Figure 4**a, the stack of OPV cells is shown.

The typical current-voltage (*I*–*V*) curves are shown in Figure 4c, and the resulting parameters are listed in **Table 3**. J_{SC} values in this work have been measured with a mask to minimize side effects for accurate results,[31] meaning that there is negligible waveguided light or extended electrode area by conductive transport layers. Despite the lower work functions of the ZnO series (4.3-4.5 eV) compared to ITO (4.7 eV) as shown in Table 2, using molecular doping in transport layers results in ohmic contacts and the same V_{OC} of 0.71 V without any injection problems for all devices. The power conversion efficiency (PCE) of the ITO reference device is 3.7% with a J_{SC} of 9.6 mA cm^{-2} and a FF of 54.6%. It is observed that ZnO-based OPV cells exhibit higher J_{SC}, FF, and PCE compared to the reference ITO device. The $OPV_{ZnO:Al,H,F}$ cell exhibits a highest PCE of 4.4% with a J_{SC} of 10.7 mA cm^{-2} and a FF of 58.3%, showing a great improvement of PCE by a factor of 1.2, when compared to the ITO-based device. To the best of our knowledge, the efficiency enhancement is the largest reported for OPV cells with alternative electrodes. Alternative electrode-based OPV cells typically show lower or comparable PCEs to the ITO reference device but they do not significantly exceed it in literature.[3–6,27,32] Especially replacing ZnO electrodes with ITO is far challenging for polymer solar cells based on PEDOT:PSS hole transport layers which show reduced PCEs compared to the ITO reference device.[8,9,13,32] It is worth mentioning that a similar enhancement to our results is observed only for intentionally textured substrates for efficient light trapping prepared by lithography, laser structuring, or chemical etching process.[33–37]

External quantum efficiency (EQE) spectra of the different cells are shown in Figure 4d. The $OPV_{ZnO:Al,H,F}$ cell shows an enhanced EQE in the wavelength of 400–700 nm, when compared with that of the OPV_{ITO} cell. This enhancement is especially pronounced at ≈530 and 630 nm. This enhanced EQE is attributed to the low optical absorption loss of the ZnO electrode series with hydrogen and fluorine co-dopants. In addition, the lower refractive index of the ZnO:Al,H,F film ($n \approx 1.8$, at 500 nm) compared to ITO ($n \approx 1.94$, at 500 nm) is acting as improvement factor. The ZnO:Al,H,F film with lower refractive index reduces the reflection of in-coming light at the interface of glass ($n \approx 1.5$)/electrode, and the electrode/organic layers ($n \approx 1.8$) due to good refractive index match.

The main differences between the ITO and ZnO electrodes used are the optical and morphological properties since the sheet resistances are kept at a similar level. At the major absorption peaks of F4-ZnPc (630 nm) and C_{60} (450 nm), the ZnO:Al,H,F film shows around 1.06 and 1.05 times higher transmittances than ITO, respectively. The J_{SC} of the $OPV_{ZnO:Al,H,F}$ cell is improved by a factor of 1.11 and the FF is also improved, compared to the ITO reference. Thus, the better transmittance alone cannot fully explain the observed performance improvement

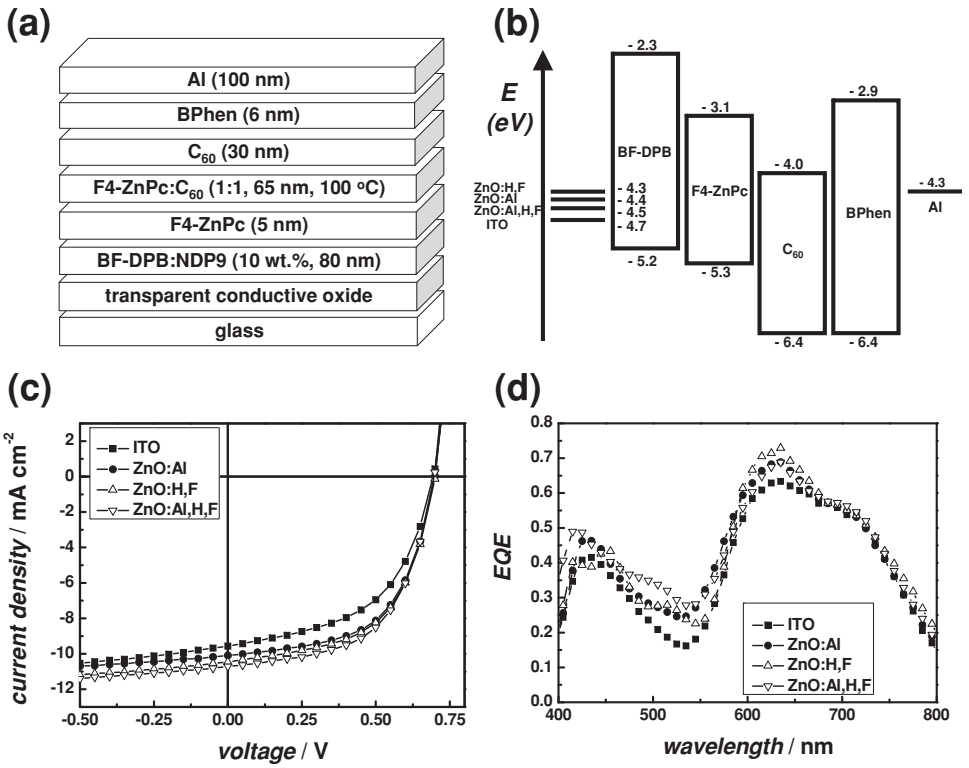

Figure 4. a) Schematic of the structure, b) energy level diagram, c) *I–V* curves, and d) EQE spectra of OPV cells with different types of bottom electrodes such as ITO, ZnO:Al, ZnO:H,F, and ZnO:Al,H,F. Enhanced J_{SC} and EQE are observed for the $OPV_{ZnO:Al,H,F}$ cell due to excellent optical properties of the optimized bottom electrode.

Table 3. The characteristics of OPV cells with different types of bottom electrodes. The PCE of the $OPV_{ZnO:Al,H,F}$ cell is improved by a factor of 1.2 compared to that of the OPV_{ITO} cell. The improved J_{SC} and FF are attributed to the optical and morphological effects of the bottom electrode.

OPV cells	V_{OC} [V]	J_{SC} [mA cm^{-2}]	FF [%]	PCE [%]
OPV_{ITO}	0.71	9.6	54.6	3.7
$OPV_{ZnO:Al}$	0.71	10.1	58.7	4.2
$OPV_{ZnO:H,F}$	0.71	10.5	57.6	4.3
$OPV_{ZnO:Al,H,F}$	0.71	10.7	58.3	4.4

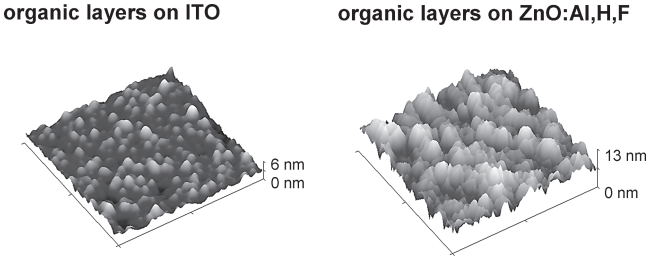

Figure 5. Topography images (1×1 μm^2) of evaporated organic layers on ITO and ZnO:Al,H,F electrodes, showing different surface topographies, caused by the underlying electrode surface structure.

in the ZnO-based OPV cells. Therefore, it is considered that a certain part of the improvement in OPV performance may stem from the surface topography. It is well known that the surface topography of electrodes and buffer layers plays a significant role in the performance of OPV cells.[33,38–43] Considering the improved FF as well as J_{SC} of the $OPV_{ZnO:Al,H,F}$ cell, it is expected that naturally structured ZnO electrodes collect charges more effectively than the flat ITO electrode, which might be due to the combined effects such as an increased contact area, shortened carrier transport distance, and desirable contact quality, enhancing J_{SC} and FF. Such an improvement of J_{SC} as well as FF by an introduction of rough metal oxide films has been reported by several groups recently.[33,38–41,43–45] To investigate the morphological effect of the electrode topography on the device performance, AFM measurements are carried out on the top organic layers of the OPV cells (**Figure 5**). It is noted that, even though relatively thick organic layers (≈186 nm) are deposited on the bottom electrodes, the surface of the organic film is different and still reflects the effect of the original electrode topography. The organic surface of the ITO reference cell shows small grains with diameters of several tens of nanometers. In contrast, the $OPV_{ZnO:Al,H,F}$ cell shows large organic structures. These results clearly demonstrate that the structures of the organic thin films and the back metal reflector are influenced by the original bottom electrode surface. Thus, the nanostructure in the absorber blend (F4-ZnPC:C_{60}) and the adjacent (C_{60}) layers are probably changed. The same applies for the back electrode, which probably reflects light more diffusively, due to the increased roughness.

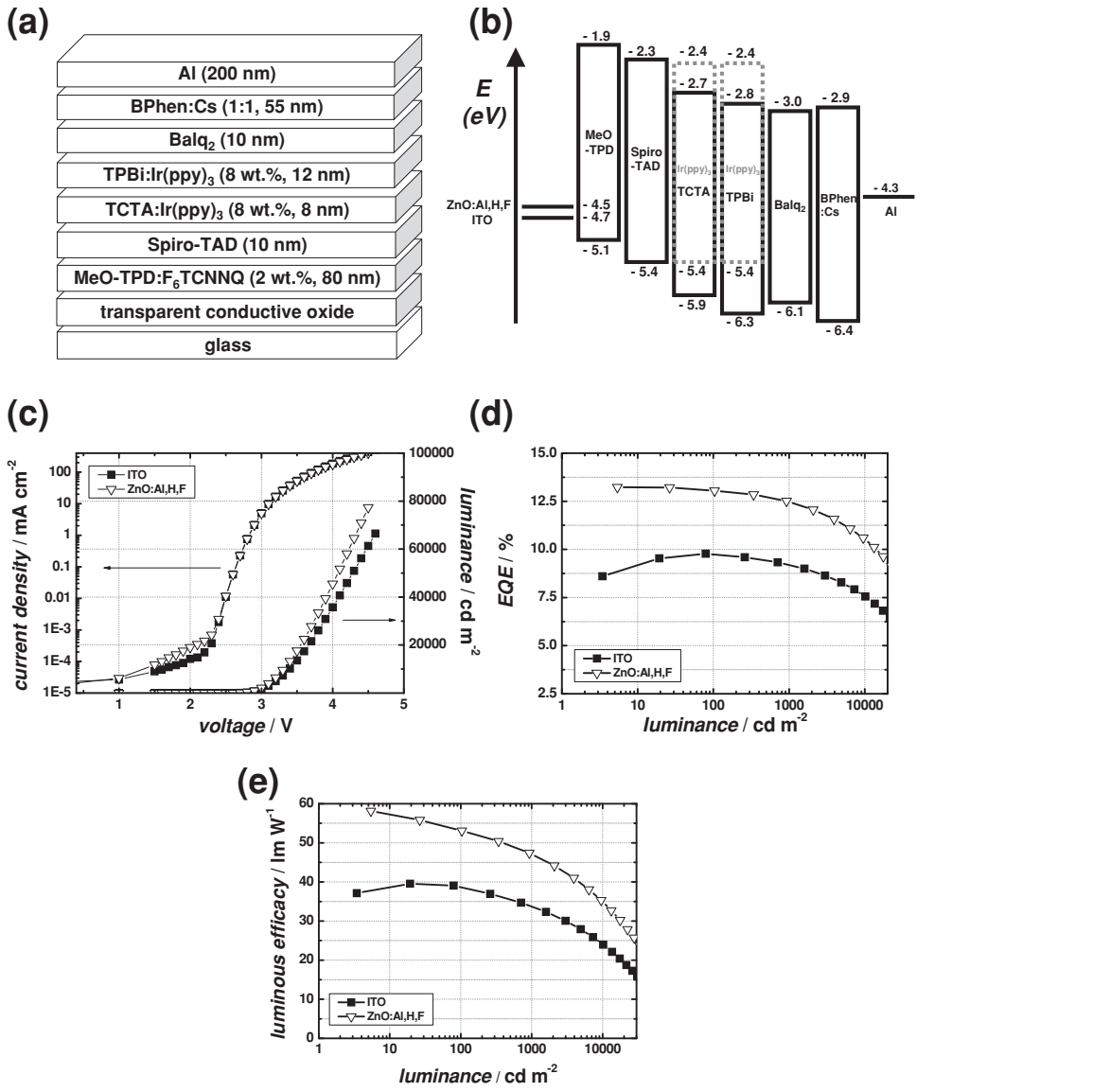

Figure 6. a) Schematic of the structure, b) energy level diagram, c) *I–V–L* curves, d) EQE, and e) luminous efficacy versus luminance of OLEDs based on ITO or ZnO:Al,H,F electrodes. The OLED with ZnO:Al,H,F exhibits improved EQE and luminous efficacy.

The outstanding optical properties of the ZnO:Al,H,F film are expected to improve the performance of OLEDs as well. Thus, we fabricate phosphorescent green OLEDs based on ITO and ZnO:Al,H,F electrodes. The OLEDs stack is visualized in **Figure 6**a. Figure 6c shows typical *I–V–L* curves for OLEDs. The *I–V* behavior of both devices is nearly equal due to similar sheet resistances of electrodes. In addition, as observed for the solar cells, the work function difference of the electrodes barely affects the electrical performance of the OLEDs due to the use of doped HTLs as shown in the *I–V* curves. For example, the onset voltages of both OLEDs are equal at 2.5 V. Figure 6d,e show the EQE and luminous efficacy (LE) of OLEDs with respect to luminance. The OLED with ZnO:Al,H,F exhibits an enhanced EQE compared to the reference ITO-based OLED. The EQE of the ITO-based OLED is 9.1% at a luminance of 1000 cd m^{-2}, while it is improved to 12.5% with the OLED on ZnO:Al,H,F by a factor of 1.4. As the *I–V* behavior for both devices is almost identical, it is clear that the enhancement is mainly attributed to the improvement of light out-coupling. A nearly matched refractive index between ZnO:Al,H,F and organic layers reduces the total internal reflection of light at the interface of electrode and organic layers. In addition, the lower optical losses of the ZnO:Al,H,F electrode allow to extract more light compared to ITO. Thus, the combined optical benefits of ZnO:Al,H,F enhance the performance of the OLEDs.

3. Conclusions

In summary, ZnO thin films are successfully optimized by co-doping of hydrogen and fluorine dopants for high optical and electrical performance as electrode materials for ITO-free OPV

cells and OLEDs. The highly transparent ZnO electrodes with hydrogen and fluorine co-dopants lead to highly improved J_{SC} and FF of OPV cells. Due to combined optical and morphological effects, caused by the naturally rough surface texture of the ZnO electrodes, a large improvement approaching 20% is possible. The enhancement factor is among the highest values reported for ITO-free OPV cells. Furthermore, the application of the same optically optimized ZnO electrodes is possible for OLEDs as well and shows an improved light extraction efficiency resulting from a reduction of waveguided light and optical losses in the electrodes. Molecular doping in transport layers of the devices allows using the ZnO electrodes in OPV cells and OLEDs without any charge injection/extraction problem or chemical instabilities. We believe that the electrode concept proposed here provides an important progress for achieving highly efficient, low-cost OPV cells and OLEDs in practical applications.

4. Experimental Section

Preparation and Characterization of the Electrodes: Reference ITO was purchased from Thin Film Devices Inc. ZnO thin films doped with aluminum (Al) (ZnO:Al), co-doped with hydrogen (H) and fluorine (F) (ZnO:H,F), and Al, H and F (ZnO:Al,H,F) were prepared on boronite glass substrates by using a conventional radio frequency (rf) magnetron sputtering system. The base pressure in the chamber was kept below 5×10^{-7} Torr. For all ZnO-based TCO films, the sputtering deposition was carried out at a pressure of 1 mTorr and a substrate temperature of 150 °C with an rf power of 50 W. The distance between the target and the substrate was 60 mm, and the substrate was rotated at a constant speed of 12 rpm during sputtering. Table 1 lists the ID of TCO films, the target composition, and sputter gas composition. Among the tested films, only ZnO:Al,H,F film was post-heat treated in vacuum at 300 °C for 1 h.

Film thickness was measured by a surface profilometer (KLAtencor, ASIQ) after etching away parts of the film in diluted HCl solution. The electrical resistivity, Hall mobility, and carrier concentration were obtained from the Hall-effect measurement by using a Van der Pauw method with indium contact pads at room temperature. For the optical analysis, the optical transmittance and reflectance spectra were obtained using a UV-visible spectrophotometer (Perkin Ellmer, Lambda 35). The atomic force microscopy (AFM) images were taken in tapping mode (AIST-NT Combiscope).

Fabrication and Characterization of the Organic Solar Cells: Small molecule OPV cells were prepared by thermal evaporation in a vacuum system (K. J. Lesker, U. K.). The base pressure of the chamber was kept around 10^{-8} Torr. The layer sequence of OPV cells was as follows (bottom to top): TCOs as bottom anodes/1 nm p-type dopant NDP9 (Novaled AG)/80 nm 10 wt% NDP9 doped *N*,*N*′-((diphenyl-*N*,*N*′-bis)9,9,-dimethyl-fluoren-2-yl)-benzidine (BF-DPB) as a hole transport layer (HTL)/5 nm fluorinated zinc phthalocyanine (F4-ZnPc)/65 nm mixed F4-ZnPc: fullerene C_{60} (volume ratio of 1:1) heated at 100 °C as a photoactive absorber layer/30 nm C_{60} as an additional absorber layer and electron transport layer/6 nm 4,7-diphenyl-1,10-phenanthroline (BPhen) as an exciton blocking layer/100 nm Al as a top electrode. After device fabrication, all devices were encapsulated with an additional glass. The solar cell active areas were ≈4.0 to 5.7 mm^2 measured using an optical microscope. All organic materials except dopant were purified by vacuum gradient sublimation. The NDP9 dopant has a better thermal stability and similar doping behavior in comparison with other dopants.[46] The solar cells were processed in our proven vacuum system, including reference samples, tracking of materials as well as frequent performance monitoring and comparisons, to ensure high reproducibility and significance of the samples made.

The current–voltage characteristics were measured using an automated setup with a source measurement unit (Keithley Instruments) under an AM 1.5G sun simulator (16S-003-300-AM1.5 from Solar Light Co., USA). The light intensity was monitored by a calibrated silicon photodiode, certified from Fraunhofer ISE, Germany. The values of J_{SC} were measured through an aperture, normalized to 100 mW cm^{-2}, and corrected for spectral mismatch. External quantum efficiency and specrtral mismatch factor were determined by a custom-made setup with a monochromator and a lock-in amplifier.

Fabrication and Characterization of the OLEDs: Organic layers were thermally evaporated in a vacuum chamber. The layer sequence for devices was as follows (bottom to top): ITO or ZnO:Al,H,F/80 nm (N,*N*,*N*′,*N*′-tetrakis(4-methoxyphenyl)-benzidine) (MeO-TPD):2,2′-(perfluoronaphthalene-2,6-diylidene)dimalononitrile (F_6TCNNQ) (2 wt%)/10 nm 2,2′,7,7′-tetrakis-(N,N′-diphenylamino)-9,9′-spirobifluorene (Spiro-TAD)/8 nm 4,4′,4″-tris(N-carbazolyl)-triphenylamine (TCTA):tris(2-phenylpyridine)-iridium ($Ir(ppy)_3$) (8 wt%)/12 nm 1,3,5-tris(N-phenylbenzimidazole-2-yl) benzene (TPBi):$Ir(ppy)_3$ (8 wt%)/10 nm bis(2-methyl-8-chinolinolato)-4-(phenyl-phenolato)-aluminum-(III) ($Balq_2$)/ 55 nm 4,7-diphenyl-1,10-phenanthroline (BPhen):Cs (1:1)/ 200 nm Al.

I–V–L characteristics and electroluminescence spectra were measured by an automated source-measure unit system (Keithley Instruments) and a calibrated spectrometer (CAS140CT-153, Instrument Systems GmbH). External quantum efficiencies were calibrated with the spatial emission of the devices, obtained by a spectro-goniometer setup.

Acknowledgements

Y.H.K. and J.S.K. contributed equally to this work. The authors thank O. R. Hild and C. May at Fraunhofer COMEDD for supporting the DIZEeff, S. Hofmann for discussion, and S. Sudhakar and BASF for providing the F4-ZnPc material. This work was funded by the European Union (EFRE), the Fraunhofer Gesellschaft, and the Free State of Saxony as part of the Dresdner Innovationszentrum Energieeffizienz. This work was supported partially by the Converging Research Center Program through the National Research Foundation of Korea (NRF) grant (2009-0082023) funded by the Ministry of Education, Science and Technology and by the Korea Science and Engineering Foundation (KOSEF) grant (2009-0064868).

Received: September 26, 2012
Revised: December 21, 2012
Published online: March 18, 2013

[1] Small molecule organic solar cells by Heliatek/IAPP with a certified efficiency of 12.0%, press release, January 2013; http://www.heliatek.com (accessed February 2013).
[2] Y. H. Kim, C. Sachse, M. Hermenau, K. Fehse, M. Riede, L. Müller-Meskamp, K. Leo, *Appl. Phys. Lett.* **2011**, *99*, 113305.
[3] Y. H. Kim, C. Sachse, M. L. Machala, C. May, L. Müller-Meskamp, K. Leo, *Adv. Funct. Mater.* **2011**, *21*, 1076.
[4] W. Gaynor, G. F. Burkhard, M. D. McGehee, P. Peumans, *Adv. Mater.* **2011**, *23*, 2905.
[5] J. Y. Lee, S. T. Connor, Y. Cui, P. Peumans, *Nano Lett.* **2008**, *8*, 689.
[6] M. W. Rowell, M. A. Topinka, M. D. McGehee, H. J. Prall, G. Dennler, N. S. Sariciftci, L. Hu, G. Gruner, *Appl. Phys. Lett.* **2006**, *88*, 233506.
[7] L. Gomez De Arco, Y. Zhang, C. W. Schlenker, K. Ryu, M. E. Thompson, C. Zhou, *ACS Nano* **2010**, *4*, 2865.
[8] V. Bhosle, J. Prater, F. Yang, D. Burk, S. Forrest, J. Narayan, *J. Appl. Phys.* **2007**, *102*, 023501.
[9] J. Owen, M. Son, K. H. Yoo, B. Ahn, S. Lee, *Appl. Phys. Lett.* **2007**, *90*, 033512.
[10] M. Jørgensen, K. Norrman, F. C. Krebs, *Sol. Energy Mater. Sol. Cells* **2008**, *92*, 686.

[11] T. Minami, *Semicond. Sci. Technol.* **2005**, *20*, S35.
[12] J. H. Park, S. J. Kang, S. I. Na, H. H. Lee, S. W. Kim, H. Hosono, H. K. Kim, *Sol. Energy Mater. Sol. Cells* **2011**, *95*, 2178.
[13] J. Bernède, L. Cattin, M. Morsli, Y. Berredjem, *Sol. Energy Mater. Sol. Cells* **2008**, *92*, 1508.
[14] P. K. Nayak, J. Kim, S. Chung, J. Jeong, C. Lee, Y. Hong, *J. Phys. D: Appl. Phys.* **2009**, *42*, 139801.
[15] R. G. Gordon, *MRS Bull.* **2000**, *25*, 52.
[16] J. Hu, R. G. Gordon, *MRS Proc.* **1990**, *202*, 457.
[17] I. Kim, K. S. Lee, T. S. Lee, J. Jeong, B. Cheong, Y. J. Baik, W. M. Kim, *J. Appl. Phys.* **2006**, *100*, 063701.
[18] C. G. Van de Walle, *Phys. Rev. Lett.* **2000**, *85*, 1012.
[19] C. G. Van de Walle, J. Neugebauer, *Nature* **2003**, *423*, 626.
[20] W. M. Kim, Y. H. Kim, J. S. Kim, J. Jeong, Y. J. Baik, J. K. Park, K. S. Lee, T.-Y. Seong, *J. Phys. D: Appl. Phys.* **2010**, *43*, 365406.
[21] Y. H. Kim, J. Jeong, K. S. Lee, J. K. Park, Y. J. Baik, T.-Y. Seong, W. M. Kim, *Appl. Surf. Sci.* **2010**, *256*, 5102.
[22] S. Lee, T. Lee, K. Lee, B. Cheong, Y. Kim, W. Kim, *J. Phys. D: Appl. Phys.* **2008**, *41*, 095303.
[23] A. Janotti, C. G. Van de Walle, *Phys. Rev. B* **2007**, *76*, 165202.
[24] L. Vlasenko, G. Watkins, *Phys. Rev. B* **2005**, *71*, 125210.
[25] S. Karan, B. Mallik, *J. Phys. Chem. C* **2007**, *111*, 7352.
[26] P. Sullivan, T. S. Jones, A. Ferguson, S. Heutz, *Appl. Phys. Lett.* **2007**, *91*, 233114.
[27] Z. Tang, L. M. Andersson, Z. George, K. Vandewal, K. Tvingstedt, P. Heriksson, R. Kroon, M. R. Andersson, O. Inganäs, *Adv. Mater.* **2012**, *24*, 554.
[28] B. Yu, L. Huang, H. Wang, D. Yan, *Adv. Mater.* **2010**, *22*, 1017.
[29] J. Meiss, A. Merten, M. Hein, C. Schuenemann, S. Schäfer, M. Tietze, C. Uhrich, M. Pfeiffer, K. Leo, M. Riede, *Adv. Funct. Mater.* **2012**, *22*, 405.
[30] J. Blochwitz, T. Fritz, M. Pfeiffer, K. Leo, D. Alloway, P. Lee, N. Armstrong, *Org. Electron.* **2001**, *2*, 97.
[31] V. Shrotriya, G. Li, Y. Yao, T. Moriarty, K. Emery, Y. Yang, *Adv. Funct. Mater.* **2006**, *16*, 2016.
[32] S. G. Ihn, K. S. Shin, M. J. Jin, X. Bulliard, S. Yun, Y. Suk Choi, Y. Kim, J. H. Park, M. Sim, M. Kim, *Sol. Energy Mater. Sol. Cells* **2011**, *95*, 1610.
[33] S. W. Cho, Y. T. Kim, W. H. Shim, S. Y. Park, K. D. Kim, H. O. Seo, N. K. Dey, J. H. Lim, Y. Jeong, K. H. Lee, *Appl. Phys. Lett.* **2011**, *98*, 023102.
[34] Z. Hu, J. Zhang, Y. Zhao, *Appl. Phys. Lett.* **2012**, *100*, 103303.
[35] L. Müller-Meskamp, Y. H. Kim, T. Roch, S. Hofmann, R. Scholz, S. Eckardt, K. Leo, A. F. Lasagni, *Adv. Mater.* **2012**, *24*, 906.
[36] K. S. Nalwa, J. M. Park, K. M. Ho, S. Chaudhary, *Adv. Mater.* **2011**, *23*, 112.
[37] X. Zhu, W. C. H. Choy, F. Xie, C. Duan, C. Wang, W. He, F. Huang, Y. Cao, *Sol. Energy Mater. Sol. Cells* **2012**, *99*, 327.
[38] C. Gong, H. B. Yang, Q. L. Song, C. M. Li, *Org. Electron.* **2012**, *13*, 7.
[39] J. Hu, Z. Wu, H. Wei, T. Song, B. Sun, *Org. Electron.* **2012**, *13*, 1171.
[40] D. C. Lim, W. H. Shim, K. D. Kim, H. O. Seo, J. H. Lim, Y. Jeong, Y. D. Kim, K. H. Lee, *Sol. Energy Mater. Sol. Cells* **2011**, *95*, 3036.
[41] W. H. Shim, S. Y. Park, M. Y. Park, H. O. Seo, K. D. Kim, Y. T. Kim, Y. D. Kim, J. W. Kang, K. H. Lee, Y. Jeong, *Adv. Mater.* **2011**, *23*, 519.
[42] R. Ulbricht, S. B. Lee, X. Jiang, K. Inoue, M. Zhang, S. Fang, R. H. Baughman, A. A. Zakhidov, *Sol. Energy Mater. Sol. Cells* **2007**, *91*, 416.
[43] H. K. Yu, W. J. Dong, G. H. Jung, J. L. Lee, *ACS Nano* **2011**, *5*, 8026.
[44] L. Chen, P. Wang, F. Li, S. Yu, Y. Chen, *Sol. Energy Mater. Sol. Cells* **2012**, *102*, 66.
[45] V. Shrotriya, G. Li, Y. Yao, C. W. Chu, Y. Yang, *Appl. Phys. Lett.* **2006**, *88*, 073508.
[46] P. Wellmann, M. Hofmann, O. Zeika, A. Werner, J. Birnstock, R. Meerheim, G. He, K. Walzer, M. Pfeiffer, K. Leo, *J. Soc. Inf. Disp* **2005**, *13*, 393.